Catalysis Science & Technology

COMMUNICATION

View Article Online
View Journal | View Issue

Cite this: *Catal. Sci. Technol.*, 2019, 9, 1103

Received 28th January 2019,
Accepted 14th February 2019

DOI: 10.1039/c9cy00176j

rsc.li/catalysis

Mechanistic insights into a NO_x storage-reduction (NSR) catalyst by spatiotemporal *operando* X-ray absorption spectroscopy†

Yasutaka Nagai, *[a] Akihiko Kato,[a] Masaoki Iwasaki [a] and Keisuke Kishita[b]

Spatially resolved monitoring of the catalytically active state and online catalytic activity measurements were applied to track the fast transient phenomena occurring along the axial direction of a NSR catalyst bed. This methodology clarified the distribution of stored NO_x as well as the cause of NO_x spike emission.

Lean-burn combustion engines, using fuels such as gasoline and diesel, provide greater fuel economy compared to conventional stoichiometric gasoline engines. However, the three-way catalysts used for conventional gasoline engines cannot purify NO_x in the oxygen-rich exhaust emitted from lean-burn engines. Therefore, new catalytic approaches are needed to treat the NO_x emissions from diesel and gasoline lean-burn engines.[1] This situation has encouraged the development of new catalyst technology that can reduce NO_x in excess oxygen, *i.e.*, a NO_x storage-reduction (NSR) catalyst for gasoline lean-burn engines,[2] also known as a lean NO_x trap (LNT). The NSR catalyst has been used practically in Japan in 1994.[3] However, vehicle emission standards have been gradually strengthened on a global scale, leading to a demand for further improvements in NSR performance. Therefore, studies of lean NO_x catalysts remain a challenging research task.[4,5]

Basically, NSR catalysts are precious group metals (PGMs; Pt, Rh and Pd) together with supporting oxides such as Al_2O_3 and barium oxide/carbonate as a NO_x storage material, that can promote catalytic oxidation and reduction processes (Fig. S1 in the ESI†). During the fuel-lean phase (oxygen excess), NO_x is oxidized over the precious metal, and then stored as barium nitrate by reaction with the barium storage component. However, during the short fuel-rich phase (reductive atmosphere) of catalyst regeneration, the stored NO_x is released and subsequently reduced to N_2 over the precious metal. Depending on the driving conditions, a burst of NO_x emission, often called an NO_x spike or NO_x puff, can be observed at the outlet of the catalyst bed during a rich period, because a portion of the stored NO_x is not reduced to N_2, leading to a NO_x slip at the outlet. Several studies have been conducted on the NO_x reduction mechanism, and significant progress has been made.[6–14] However, the nature of NO_x spike generation during the fast transient reaction remains very complicated, and requires further investigation.

To elucidate the NO_x spike generation mechanism, understanding the spatially resolved reactions occurring in the catalyst bed is necessary, because chemical species and catalytic active states have drastic gradients along the axial direction of the catalyst bed. Several research groups have conducted spatially resolved analysis of the NSR process using infrared (IR)/Raman spectroscopy that provides surface and bulk information about the Ba species,[6–9] spatially resolved capillary-inlet mass spectrometry (SpaciMS) to monitor the composition of the gas phase,[10–13] and IR thermography to obtain temperature measurements.[14] Spatial analysis of the PGM active site is vitally important to understand the NSR process in the entire catalyst bed from front to rear. However, no studies have ever been conducted to track the PGM active state in the axial direction of the NSR catalyst. This is because the oxidation–reduction rate of the PGM, which is related to the catalytically active state, is very fast under the lean/rich perturbations at temperatures of about 200 °C and above,[15,16] therefore, fast *operando* analysis methodology with millisecond temporal resolution is required to track the PGM active state.

Therefore, a spatiotemporal *operando* X-ray absorption spectroscopy (XAS) method was applied to obtain spatially resolved monitoring of PGM in the axial direction as well as for the measurement of online outlet gas components to clarify the NO_x storage and reduction processes, especially the NO_x spike mechanism. A Toyota beamline (BL33XU) of SPring-8, combining a servo-motor-driven Si channel-cut

[a] *Toyota Central R&D Labs., Inc., Nagakute, Aichi 480-1192, Japan. E-mail: e1062@mosk.tytlabs.co.jp*
[b] *Toyota Motor Corporation, Toyota, Aichi 471-8572, Japan*

† Electronic supplementary information (ESI) available. See DOI: 10.1039/c9cy00176j

monochromator with a tapered undulator, allowed rapid acquisition of high-quality data for quick scan XAS (QXAS),[17] along with an *operando* setup simulating automotive engine exhaust (Fig. S2a†). This study presents the importance of *operando* spatiotemporally resolved QXAS analysis for heterogeneous catalytic processes, and reveals the nature of the NO_x storage and reduction process.

In this study, a 0.5 wt% Rh/BaO (10 wt% as Ba)/γ-Al_2O_3 catalyst was prepared. A capillary tube with a pellet catalyst sample (66 mg, sieve fraction 75–150 μm, *ca.* 8 mm in catalyst bed length) was set in a specially designed *operando* cell (Fig. 1a and b). The NSR reaction was operated at 450 °C, and a lean stream consisting of 0.07% NO, 7% O_2, and He balance was introduced into the cell for 300 or 60 s, followed by a rich stream of 3% H_2 and He balance for 240 s. The gas flowing over the sample was quickly changed from a lean to a rich atmosphere using a gas-actuated switching valve (Fig. S2b†). Measurement of inlet/outlet NO concentration confirmed that the amount of stored NO_x during the lean 60 s supply corresponded to 0.050 mmol per g of catalyst (33% of the saturated NO_x storage amount) and that during the lean 300 s supply, the amount corresponded to 0.151 mmol per g of catalyst (100% NO_x storage amount). The experiments of 300 s and 60 s of lean supply are referred to as 100% and 33% NO_x storage, respectively. Under the NSR operation, online mass spectra of the outlet gas species were obtained every 150 ms, along with XAS measurements.

To track the catalytically active state, Rh K-edge X-ray absorption near-edge structure (XANES) spectra were collected every 100 ms at four positions: 1 (A), 3 (B), 5 (C), and 7 (D) millimeters from the bed front (Fig. 1a). High-quality data from the Rh K-edge XANES spectra were acquired using QXAS in transmission mode (Fig. S2c†), which enabled tracking of temporal changes in the Rh oxidation state as Rh metal fraction. Fig. 1c and d show the Rh metal fraction at each position (A–D) after switching from lean gas to rich gas at 450 °C.

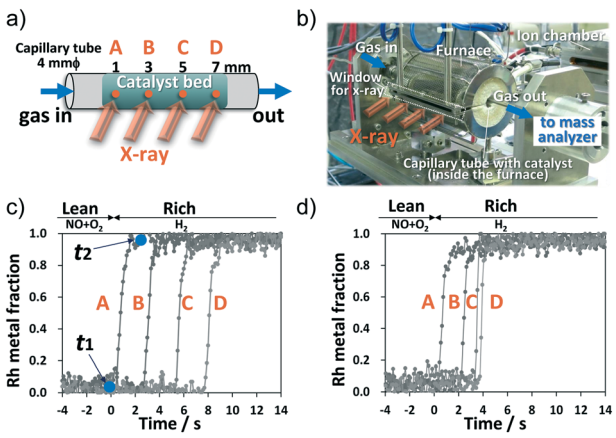

Fig. 1 (a) Schematic illustration of the quartz capillary tube with the pellet catalyst. (b) The *operando* XAS cell for spatially-resolved analysis in the axial direction. Temporal dependence of the Rh metal fraction in the Rh/BaO/Al_2O_3 catalyst from lean to rich conditions for (c) 100% NO_x storage and (d) 33% NO_x storage.

Under the lean conditions, all Rh species in the catalyst bed were Rh oxide (Rh_2O_3). After switching to the rich condition, for both 100% and 33% NO_x storage, reduction in Rh occurred sequentially from the front A position to the rear D position. Thus, Rh at the downstream position (*e.g.*, position B) was not reduced unless the reduction in Rh upstream (*e.g.*, position A) was completed. The metallic Rh state is considered an active state for catalytic NO reduction[18–20] because Rh metallic clusters are required for the NO dissociation step. This indicates that NO reduction with H_2 over the Rh species occurred sequentially from upstream to downstream.

In Fig. 1c, "*t*1" and "*t*2" denote the onset time and the termination time, respectively, of Rh reduction, and the value obtained by subtracting *t*1 from *t*2 is defined as the "Rh reduction time" (calculation method in Fig. S3†). Fig. 2a presents the Rh reduction time at each axial position for 100% and 33% NO_x storage along with that for 0% NO_x storage. The 0% NO_x storage conditions were for the experiment conducted under a lean stream of only 7% O_2/He (without the NO gas component) for 300 s and then a rich stream of 3% H_2/He for 240 s at 450 °C. Temporal dependencies of the Rh metal fraction at each position for 0% NO_x storage are shown in Fig. S4.† In Fig. 2a, the NO_x reduction time for 33% NO_x storage at each axial position varied widely from 1.2 s at A to 0.2 s at D, whereas those of 100% and 0% NO_x storage produced constant values (1.1–1.2 s for 100% storage and ~0.2 s for 0% storage). These results indicate that the Rh reduction time correlates with the amount of stored NO_x. As shown in Fig. S5,† the greater the amount of stored NO_x, the longer the Rh reduction time because the stored NO_x prolongs the reduction of Rh oxide. Thus, the Rh reduction time during the rich period was proportional to the amount of NO_x stored in the Ba compounds in the lean period. Results shown in Fig. 2a clearly indicate that NO_x is fully stored

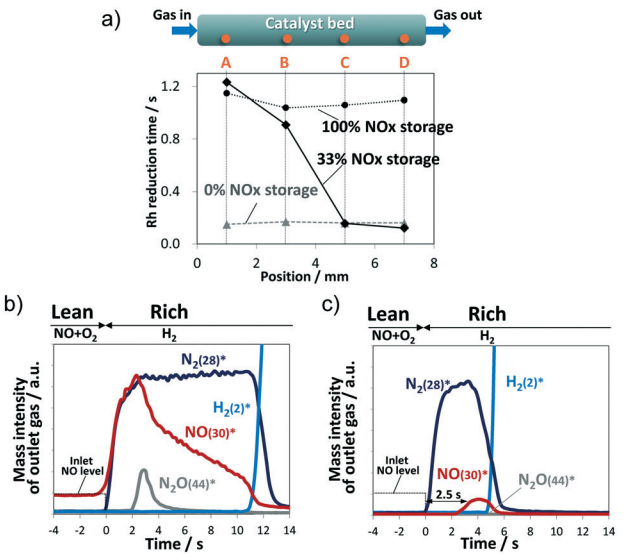

Fig. 2 (a) Rh reduction time at each axial position. Evolution profiles of the outlet gases for (b) 100% NO_x storage and (c) 33% NO_x storage, **m*/*z* is given in the parentheses.

along the entire length of the catalyst bed after 300 s of lean supply (100% NO_x storage), whereas for 33% NO_x storage, NO_x is stored only upstream at the A and B positions.

Fig. 2b shows the evolution profiles of outlet NO, N_2, N_2O, and H_2 gases when the gas flow was switched from lean to rich conditions at 100% NO_x storage. NH_3 production was not observed within the measurement time in Fig. 2b. After switching to the rich period of H_2/He flow, a spike in NO emission was observed along with N_2 generation from the reaction of H_2 with the stored NO_x, indicating that the stored NO_x decomposed during the rich period to gas phase NO_x and was subsequently released to the outlet of the catalyst bed without being reduced to N_2. Such NO emission lasted for about 11 s until unreacted H_2 was evolved.

In addition to N_2 as a NO_x reduction product, a trace amount of N_2O was confirmed at around 3 s. Kubiak *et al.* investigated mechanistic aspects in the formation of N_2O over $Pt/BaO/Al_2O_3$ and $Rh/BaO/Al_2O_3$ by transient microreactor experiments and *operando* IR spectroscopy.[21] They concluded that N_2O formation involves the coupling of gaseous NO molecules with N-adspecies formed upon NO dissociation onto PGM sites. As for 100% NO_x storage in our experiment, it is reasonable to consider that the concentration of gas phase NO became the highest at around 3 s, and trace N_2O was generated accordingly.

The gas atmosphere along the axial direction inside the catalyst bed during the rich period was investigated. Since the reduction reaction rate of stored NO_x is sufficiently faster than the gas flow velocity, NO reduction at the Rh metal sites proceeded sequentially from the upstream position with complete consumption of H_2. Actually, at the elapsed time of 1 s (Fig. 1c), the Rh species at position A is reduced, but the Rh species in the region from position B to D remain as Rh oxide. Considering that the time for gas to flow through the catalyst bed was 60 ms for this experiment, the downstream region from B to D, after H_2 was completely consumed at the upstream of position A, is basically under an inert gas atmosphere (He plus N_2). A schematic for this process is shown in Fig. S6.†

Luo *et al.*[11] and Choi *et al.*[13] reported that the stored NO_x during a lean period is released to the outlet of the catalyst bed as gaseous NO_x during an inert gas purge at temperatures of 400 °C and above. In addition, Luo *et al.*[11] reported that an oxidizing atmosphere (oxygen excess) stabilizes barium nitrates, whereas they become less stable under an inert gas atmosphere, resulting in the formation of a NO_x puff. Urakawa *et al.*[6] investigated the dynamic surface and bulk processes of Ba components during NSR reactions using spatiotemporal IR/Raman spectroscopy. Their results suggested that the surface Ba nitrite species decomposed during the rich period, releasing NO into the gas phase. According to their investigation, a portion of stored NO_x in the region from B to D in this study became unstable under the inert gas atmosphere and was released to the outlet as a NO_x spike emission.

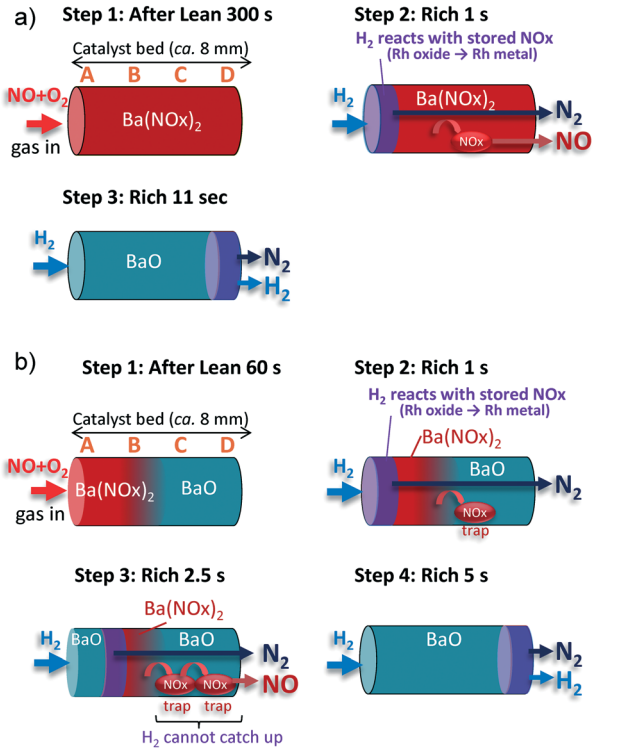

Fig. 3 Schematic illustration of NO_x storage and reduction behavior for (a) 100% NO_x storage and (b) 33% NO_x storage.

All of these results led to the following conclusions about the NSR process for 100% NO_x storage (Fig. 3a):

Step 1: After the lean period of 300 s, NO_x is fully stored along the entire length of the catalyst bed as barium nitrite or barium nitrate [$Ba(NO_x)_2$)].

Step 2: During the first second of the rich period, the stored NO_x at the front position near A is reduced to N_2 by H_2 over the metallic Rh species, and N_2 is released to the outside of the catalyst bed. At the same time, a portion of the stored NO_x at the back position of B–D (*e.g.*, the surface nitrites which are weakly adsorbed) is decomposed under the inert gas, and released into the gas phase. Therefore, NO spike emission and N_2 generation begin to occur almost simultaneously. Besides, a trace amount of N_2O is generated in the presence of gas phase NO at around 3 s.

Step 3: Step 2 continues for ~11 s until H_2 reaches the end of the catalyst bed. At this point, all of the stored NO_x is reduced by H_2, which is consistent with the termination of Rh reduction at position D (Fig. 1c).

Next, the 33% NO_x storage case was examined by obtaining outlet gas profiles (Fig. 2c). The amount of N_2 generation from 33% NO_x storage (0.024 mmol g^{-1}) was less than that for the 100% NO_x storage case (0.059 mmol g^{-1}), by a value that corresponds to the difference between the two NO_x storage amounts (0.050 and 0.151 mmol g^{-1}). H_2 emission was observed at approximately 5 s into the rich period, which is consistent with the time when reduction of Rh species at position D was completed (Fig. 1d). Note the delay of 2.5 s

for NO emission after N_2 generation in the 33% NO_x storage case. A similar delay was not observed for 100% NO_x storage.

The delay of the NO spike was investigated (Fig. S7†). According to the Rh reduction behavior in Fig. 1d during the first second of the rich period, a H_2 atmosphere exists upstream of position A; in contrast, the atmosphere downstream from B to D contains an inert gas. The NO_x stored near position B under the inert gas is decomposed to the gas phase, resulting in desorbed NO_x flowing downstream relatively slowly because the gas phase NO_x is weakly trapped in the downstream C and D regions at vacant sites on the BaO surface. This slow travel *via* repetition of desorption/re-trapping results in a 2.5 s delay based on the onset time of N_2 emission.

Incidentally, the ratio of the NO_x spike emission amount to the amount of stored NO_x for 33% NO_x storage, calculated from the evolution profiles of the outlet gases (Fig. 2c), was 4%, which is significantly less than the 21% found for 100% NO_x storage (Fig. 2b). This difference is interpreted as follows. Since no re-trap sites are available downstream in the 100% NO_x storage case, the decomposed NO_x exits unreduced from the catalyst bed. In contrast, for the 33% NO_x storage case, some of the downstream re-trapped NO_x species are reduced to N_2 at the Rh sites by H_2 coming from upstream, and the travelling NO_x species that the H_2 does not reach are released to the outlet.

Thus, the NSR process for 33% NO_x storage is interpreted as follows (Fig. 3b):

Step 1: After the 60 s lean period, NO_x is stored as $Ba(NO_x)_2$ upstream of the A and B positions. Downstream, from C to D, vacant sites (BaO) exist for NO_x trapping.

Step 2: During the first second of the rich period, the NO_x stored at the front position near A is reduced to N_2 by H_2 over the metallic Rh species, and released to the outside. At the same time, a portion of the NO_x stored toward the back of B is decomposed under the inert gas and released into the gas phase. The decomposed NO_x species are re-trapped downstream in the C and D regions.

Step 3: At 2.5 s into the rich period, the reduction front reaches position B. The decomposed NO_x species travel farther downstream, repeating the desorption/re-trap process on the vacant sites. The traveling NO_x is released to the outlet as an NO spike unless H_2 gas reaches the traveling NO_x.

Step 4: Step 3 continues until the H_2 reaches the D position, and then H_2 emission is observed at approximately 5 s into the rich period.

Conclusions

A spatiotemporal *operando* XAS technique was used to investigate the dynamic behavior of the NO_x storage and reduction process of a $Rh/BaO/Al_2O_3$ catalyst. The Rh K-edges XAS in the axial direction of the catalyst bed were monitored every 100 ms, which was combined with online mass spectrometry. Using this methodology, the fast transient phenomena occurring inside the NSR catalyst were tracked and the NO_x storage distribution during the lean period was clarified, along with the cause of the NO_x spike emission.

In this study, a simplified model gas containing NO + O_2 and H_2 was used, in order to gain mechanistic insights into the principal NSR process. However, an actual engine exhaust includes H_2O, CO_2, CO and so on. Using the spatiotemporal *operando* XAS methodology, we plan to investigate the effect of coexisting gases and reductants on the catalytic active site. Furthermore, combining SpaciMS with the current XAS set-up can give a deeper understanding of the overall mechanism occurring in the NSR convertor. We hope to establish an ultimate spatiotemporal *operando* system in the near future.

Conflicts of interest

There are no conflicts to declare.

Acknowledgements

The authors are grateful to Kazuhiko Dohmae, Toshitaka Tanabe, and Hideki Takagi (Toyota Central R&D) for their helpful discussions and excellent support.

Notes and references

1 A. Fritz and V. Pitchon, *Appl. Catal., B*, 1997, **13**, 1.
2 N. Takahashi, H. Shinjoh, T. Iijima, T. Suzuki, K. Yamazaki, K. Yokota, H. Suzuki, N. Miyoshi, S. Matsumoto, T. Tanizawa, T. Tanaka, S. Tateishi and K. Kasahara, *Catal. Today*, 1996, **27**, 63.
3 S. Matsumoto, *Catal. Today*, 1996, **29**, 43.
4 T. C. Waltling, P. D. Bolton and D. Swallow, *Chem. Eng. Sci.*, 2018, **178**, 312.
5 X. Mei, Q. Yan, P. Lu, J. Wang, Y. Cui, Y. Nie, A. Umar and Q. Wang, *Sci. Rep.*, 2017, **7**, 42862.
6 A. Urakawa, N. Maeda and A. Baiker, *Angew. Chem., Int. Ed.*, 2008, **47**, 9256.
7 N. Maeda, A. Urakawa and A. Baiker, *Top. Catal.*, 2009, **52**, 1746.
8 N. Maeda, A. Urakawa and A. Baiker, *J. Phys. Chem. C*, 2009, **113**, 16724.
9 N. Maeda, A. Urakawa, R. Sharma and A. Baiker, *Appl. Catal., B*, 2011, **103**, 154.
10 J. Choi, W. P. Partridge and C. S. Daw, *Appl. Catal., A*, 2005, **293**, 24.
11 J. Y. Luo, M. Alharbi, M. Pang and W. S. Epling, *Appl. Catal., B*, 2011, **106**, 664.
12 V. Easterling, Y. Ji, M. Crocker, M. Dearth and R. W. McCabe, *Appl. Catal., B*, 2012, **123–124**, 339.
13 J. S. Choi, W. P. Partridge, J. A. Pihl, M. Y. Kim, P. Kočí and C. S. Daw, *Catal. Today*, 2012, **184**, 20.
14 K. Aftab, J. Mandur, H. Budman, N. W. Currier, A. Yezerets and W. S. Epling, *Catal. Lett.*, 2008, **125**, 229.
15 K. Dohmae, Y. Nagai, T. Tanabe, A. Suzuki, Y. Inada and M. Nomura, *Surf. Interface Anal.*, 2008, **40**, 1751.

16 J. D. Grunwaldt, M. Beier, B. Kimmerle, A. Baiker, M. Nachtegaal, B. Grisesebock, D. Lutzenkrichen-Hecht, J. Stotzel and R. Frahm, *Phys. Chem. Chem. Phys.*, 2009, **11**, 8799.
17 T. Nonaka, K. Dohmae, T. Araki, Y. Hayashi, Y. Hirose, T. Uruga, H. Yamazaki, T. Mochizuki, H. Tanida and S. Goto, *Rev. Sci. Instrum.*, 2012, **83**, 083112.
18 J. Evans and M. Tromp, *J. Phys.: Condens. Matter*, 2008, **20**, 184020.
19 A. J. Dent, J. Evans, S. G. Fiddy, B. Jyoti, M. A. Newton and M. Tromp, *Faraday Discuss.*, 2008, **138**, 287.
20 H. Asakura, S. Hosokawa, T. Ina, K. Kato, K. Nitta, K. Uera, T. Uruga, H. Miura, T. Shishido, J. Ohyama, A. Satsuma, K. Sato, A. Yamamoto, S. Hinokuma, H. Yoshida, M. Machida, S. Yamazoe, T. Tsukada, K. Teramura and T. Tanaka, *J. Am. Chem. Soc.*, 2018, **140**, 176.
21 L. Kubiak, R. Matarrese, L. Castoldi, L. Lietti, M. Daturi and P. Forzatti, *Catalysts*, 2016, **6**, 36.